

Eddy Amplitudes in Baroclinic Turbulence Driven by Nonzonal Mean Flow: Shear Dispersion of Potential Vorticity

K. SHAFER SMITH

Center for Atmosphere Ocean Science, Courant Institute of Mathematical Sciences, New York University, New York, New York

(Manuscript received 13 April 2006, in final form 17 July 2006)

ABSTRACT

As in the midlatitude atmosphere, midocean eddies are primarily generated by baroclinically unstable mean currents. In contrast to the atmosphere, however, oceanic currents are significantly nonzonal. Even weak nonzonal currents are linearly unstable since β does not suppress growing meridional waves. Theories for the nonlinear equilibration of baroclinic instability, and hence theories for the amplitudes of midocean eddies, must therefore take into account the different dynamics of nonzonal flow. It is shown here that the amplitude of fully developed baroclinic turbulence due to nonzonal shears differs from that due to zonal shears primarily in the nature of the eddy generation. Since β will act to create large-scale zonal jet structures regardless of the generation source, the nature of eddy fluxes of potential vorticity (the source of eddy energy) in the zonal and meridional directions are fundamentally different. The cross-jet mixing has been shown previously to obey a mixing-length scaling, and this corresponds to the generation due to unstable zonal flow. The along-jet mixing, which corresponds to the generation due to the meridional shear, is shown here to be best described by a shear dispersion model. The resulting flux is orders of magnitude higher than in the cross-jet direction, and thus eddy energies driven by baroclinically unstable mean flows with a nonzero meridional component are much larger. This provides an explanation for recently reported results. Moreover, given recent observational and modeling studies showing the ubiquitous presence of zonal jets in the oceans, the results presented here indicate a powerful source of eddy energy.

1. Introduction

Continental boundaries lead to a mean oceanic stratification with both zonal and meridional structure, so by thermal wind balance local mean flows can take on any direction—this situation can be contrasted with the atmosphere in which the mean winds are primarily zonal. Midlatitude storm tracks have long been associated with baroclinic instability of that zonal mean flow (Charney 1947), and much of the theory, both linear and nonlinear, of baroclinic instability has been developed for vertically sheared zonal mean flow. Baroclinic instability of vertically sheared meridional mean flow is well understood from a linear perspective (Robinson and McWilliams 1974; Pedlosky 1987; Walker and Pedlosky 2002); the essential distinction from zonal theory is that arbitrarily weak meridional shear can lead to

growing waves because the northward Coriolis gradient (β) does not prevent sign changes of the mean zonal potential vorticity gradient. In practical terms, this means that the oceanic available potential energy stored in east–west gradients of the pycnocline is more easily converted to eddy kinetic energy than that stored in north–south gradients.

The turbulence resulting from the baroclinic instability of a vertically sheared meridional current, on the other hand, has only recently been investigated. Spall (2000) and Arbic and Flierl (2004a) find that steady-state eddy energies generated by this mechanism can exceed the mean kinetic energy by more than a factor of 1000, much in excess of eddy energies obtained in simulations of zonally generated baroclinic instability (e.g., Held and Larichev 1996). Thus not only are east–west gradients of density surfaces more unstable, but the ensuing turbulence results from an extreme amplification of the transfer from mean to eddy energy. One goal of Spall (2000), and the primary goal of the present paper, is to understand the eddy generation mechanism and nonlinear equilibration in nonzonal baroclinic tur-

Corresponding author address: K. Shafer Smith, Center for Atmosphere Ocean Science, New York University, 251 Mercer Street, New York, NY 10012.
E-mail: shafer@cims.nyu.edu

bulence and to find a theory for their dependence on mean flow parameters. Given the ubiquity of meridional flow in the ocean, a closed theory for these statistics is a necessary component of any successful potential-vorticity-based ocean eddy parameterization.

Spall (2000) considers baroclinic turbulence driven by nonzonal mean flows in a series of simulations, using both a meridional channel and a wind-driven basin, and provides a theory that successfully describes the scaling of the obtained eddy energies with the parameters of the problem. The theory derived depends critically on the zonal width of the domain, which is assumed to set the length scale in a diffusive closure for the eddy potential vorticity flux (the details will be reviewed in the next section). The implication is that the width of the basin sets the zonal eddy scales that result from nonzonal baroclinic instability in the real ocean and, by extension, that “local” theories for midocean eddy statistics are inapplicable. In other words, the theory implies that the “homogeneous limit” of Haidvogel and Held (1980) does not really exist.

Arbic and Flierl (2004a), on the other hand, investigate baroclinic turbulence driven by nonzonal flows in a doubly periodic model, where no domain scale is present. They find that eddy energies do saturate but that the equilibrated energy level is very sensitive to bottom drag, and moreover increases with increasing β , just the opposite of the trend predicted by Spall’s theory. It is also opposite the trend for zonal baroclinic instability in which eddy energy decreases with increasing β (e.g., Held and Larichev 1996). The fact that a steady state is obtained in these experiments implies that, in lieu of boundaries or zonal inhomogeneities, some local mechanism must act to set the zonal eddy length scale.

The complexity of the boundary-free problem must lie in understanding the effects of the mean vorticity gradient, β . Were it not for β , the eddy flow would be isotropic and there could be no statistical dependence on the mean flow direction. The linear theory leads one to consider the effects of β on suppressing the linear instability, but in fully developed turbulence β has a second, unrelated effect on the flow: the inverse cascade of energy produced by baroclinic instability is impeded in the meridional direction by the Rossby dispersion relation, leading to the formation of zonal jets (Rhines 1975; Williams 1978; Vallis and Maltrud 1993). A slew of recent papers (Maximenko et al. 2005; Richards et al. 2006; Nadiga 2006) have revealed the presence of jets in both ocean observations and numerical models. How does this eddy anisotropy affect the energy levels in nonzonal baroclinic turbulence?

Eddy energy generation by baroclinic instability is proportional to the eddy flux of eddy potential vorticity,

$$\frac{dE}{dt} = \int_{-H}^0 (\overline{Vu'q'} - \overline{Uv'q'}) dz - \text{dissipation}, \quad (1.1)$$

where the overbar represents a horizontal spatial average (assuming homogeneous statistics), H is the depth, E is the eddy energy, $\mathbf{U} = \bar{\mathbf{u}} = U(z)\mathbf{i} + V(z)\mathbf{j}$ is the mean velocity, $\mathbf{u}' = u'(x, y, z, t)\mathbf{i} + v'(x, y, z, t)\mathbf{j}$ is the eddy velocity, and q' is the eddy quasigeostrophic potential vorticity (PV). In the classic problem, $V = 0$ and, when the zonal shear is unstable, the generation is due to the northward eddy flux of eddy potential vorticity. When the turbulence is either isotropic or zonally elongated, v' is random and uncorrelated, and $\overline{v'q'}$ turns out to be well approximated by a mixing-length hypothesis and downgradient mixing of potential vorticity (Larichev and Held 1995; Held and Larichev 1996; Smith and Vallis 2002).

In the special case that $U = 0$, however, one can see from (1.1) that the generation will be driven by correlations between the zonal eddy flow and the eddy PV. When the eddies are zonally elongated or jetlike, u' is coherent and there is no reason to expect a mixing length hypothesis to describe the eastward flux of eddy PV. Rather, for scales large compared to the deformation scale, the PV is primarily baroclinic, and its flux is primarily due to passive advection by barotropic eddies (Salmon 1980). In this case, one should consider the transport of a passive scalar by jet flow in a turbulent background. Particle pairs will be sheared apart, but will remain correlated over large flight distances, until randomness in the turbulent background decorrelates them. Thus the weaker the background turbulent diffusion, the larger the effective along-jet transport. This is the shear dispersion problem first described by Taylor (1953), and the quantitative result is that the flux along the jet is inversely proportional to the background diffusivity. When the background diffusion is due to turbulent mixing, the diffusivity can be related to the across-jet flux.

The specific application of shear dispersion to the flux of a tracer by β -plane jet flow is worked out in Smith (2005). It is shown in the present paper that a shear dispersion model for the flux of eddy potential vorticity is sufficient to explain the trends and high energy levels found by Spall (2000) and Arbic and Flierl (2004a) for nonzonal baroclinic turbulence. Specifically, because the cross-jet flux decreases with increasing β , the along-jet flux does just the opposite, so the energy generation increases with increasing β (so long

as the eddy flow is zonally elongated, which can be prevented if the bottom drag is strong enough). The present theory falls short, however, of providing a complete closure for the problem. An intensely nonlinear feedback mechanism makes it extremely difficult to change the jet scale in the weak drag limit, even over more than a decade of values of β . The details are described in the body of the paper.

The paper is organized as follows. The background to the problem of fully developed baroclinic turbulence driven by a nonzonal mean flow is worked out in section 2. Numerical experiments designed to explore the problem and the theory to describe the results are described in section 3. Conclusions are given in section 4.

2. Background

The quasigeostrophic (QG) approximation is appropriate for small Rossby number phenomena with length scales of order of the deformation scale, and so is an appropriate model for nonequatorial mesoscale ocean eddy dynamics. Given a background flow $\mathbf{U} = U(z)\mathbf{i} + V(z)\mathbf{j}$, assumed to be steady on eddy time scales, and set by large-scale wind and buoyancy forcing (i.e., we do not require that it be a quasigeostrophic solution), the mean streamfunction is

$$\bar{\psi} = -U(z)y + V(z)x.$$

Quasigeostrophic perturbations (dropping primes) about this mean will satisfy the potential vorticity conservation equation

$$\frac{\partial q}{\partial t} + J(\psi, q) = -\mathbf{U} \cdot \nabla q - \mathbf{u} \cdot \nabla Q + D, \quad (2.1)$$

where D represents drag and dissipation terms,

$$q = \nabla^2 \psi + \frac{\partial}{\partial z} \left(\frac{f^2}{N^2} \frac{\partial \psi}{\partial z} \right)$$

is the eddy QG potential vorticity, $N = N(z)$ is the background buoyancy frequency, f is the Coriolis parameter, and

$$\nabla Q = \frac{d}{dz} \left(\frac{f^2}{N^2} \frac{dV}{dz} \right) \mathbf{i} + \left[\beta - \frac{d}{dz} \left(\frac{f^2}{N^2} \frac{dU}{dz} \right) \right] \mathbf{j}$$

is the mean PV gradient. Multiplying (2.1) by $-\psi$ and integrating over space results in the energy generation equation (1.1) discussed in the introduction.

To address the issue at hand, we specialize to the case of two equal-depth layers. Denoting the upper and lower layer eddy streamfunctions as ψ_1 and ψ_2 , respectively, the two-layer system can be represented in terms of baroclinic and barotropic modes with barotropic

eddy streamfunction $\psi = (\psi_1 + \psi_2)/2$ and baroclinic eddy streamfunction $\tau = (\psi_1 - \psi_2)/2$. The barotropic and baroclinic eddy potential vorticities are then $q_\psi = \nabla^2 \psi$ and $q_\tau = \nabla^2 \tau - \lambda^2 \tau$, respectively, where λ is the internal deformation wavenumber (the inverse of the internal Rossby deformation radius). Assuming without loss of generality that the background velocities are purely baroclinic, with $U = (U_1 - U_2)/2$ and $V = (V_1 - V_2)/2$, and invoking a linear vorticity drag in the bottom layer, the equations of motion for this system are

$$\begin{aligned} \frac{\partial q_\psi}{\partial t} + J(\psi, q_\psi) + J(\tau, q_\tau) + \beta \frac{\partial \psi}{\partial x} &= -\mathbf{U} \cdot \nabla (q_\tau + \lambda^2 \tau) \\ &+ \frac{r}{2} \nabla^2 (\tau - \psi) + D_\psi \quad \text{and} \end{aligned} \quad (2.2a)$$

$$\begin{aligned} \frac{\partial q_\tau}{\partial t} + J(\psi, q_\tau) + J(\tau, q_\psi) + \beta \frac{\partial \tau}{\partial x} &= -\mathbf{U} \cdot \nabla (q_\psi + \lambda^2 \psi) \\ &+ \frac{r}{2} \nabla^2 (\psi - \tau) + D_\tau, \end{aligned} \quad (2.2b)$$

where D_ψ and D_τ are small-scale dissipation terms.

As originally noted by Salmon (1980), at horizontal length scales $l \gg \lambda^{-1}$ the equations (ignoring drag since here we are concerned with energy generation) can be approximated as forced two-dimensional barotropic flow advecting a passive scalar with a linear mean gradient

$$\frac{\partial q_\psi}{\partial t} + J(\psi, q_\psi) + \beta \frac{\partial \psi}{\partial x} \simeq F_\tau + D_\psi \quad \text{and} \quad (2.3a)$$

$$\frac{\partial \tilde{q}_\tau}{\partial t} + J(\psi, \tilde{q}_\tau) + \lambda^2 U y - \lambda^2 V x \simeq D_\tau, \quad (2.3b)$$

where $F_\tau = -J(\tau, q_\tau)$ can be thought of as a forcing term from the baroclinic dynamics and we have defined the approximate baroclinic PV as $\tilde{q}_\tau \equiv -\lambda^2 \tau \simeq q_\tau$.¹

To put this approximation to use, we first relate the energy generation rates to the PV transport. Multiplying (2.3a) by $-\psi$ and (2.3b) by $-\tau$ and integrating each over horizontal space and summing, one obtains the energy budget for the two-layer system

¹ The rationalization for dropping the mean flow term from the barotropic equation, equivalent to $-\mathbf{U} \cdot \nabla (\nabla^2 \tau)$, without making an explicit assumption about the magnitude of \mathbf{U} , is that it does not generate energy nor does it act to redistribute energy horizontally among wavenumbers: in a spectral energy budget, it is balanced wavenumber-for-wavenumber by its counterpart in the baroclinic equation. Since we are concerned with energy generation, transfer and dissipation, the term is not relevant.

$$\frac{dE}{dt} = -U\overline{v_\psi \tilde{q}_\tau} + V\overline{u_\psi \tilde{q}_\tau} - \overline{\psi D_\psi} - \tau \overline{D_\tau},$$

analogous to (1.1). Anticipating use of the passive scalar analogy, we define diffusivities in each direction

$$k_x = (\lambda^2 V)^{-1} \overline{u_\psi \tilde{q}_\tau} \quad \text{and} \quad \kappa_y = -(\lambda^2 U)^{-1} \overline{v_\psi \tilde{q}_\tau},$$

where we have used $\partial \overline{q_\tau} / \partial x = -\lambda^2 V$ and $\partial \overline{q_\tau} / \partial y = \lambda^2 U$. Thus the generation of eddy energy due to a gradient in the x direction is $\lambda^2 V^2 \kappa_x$ and that due to a gradient in y is $\lambda^2 U^2 \kappa_y$, which demonstrates that downgradient PV fluxes indeed generate eddy energy.

In the standard case with $V = 0$, Held and Larichev (1996) suggest an approximate closure for the eddy energy level and scale utilizing the passive scalar analogy for the baroclinic dynamics and the phenomenology of β -plane turbulence for the barotropic flow. In particular, they assume: 1) the diffusivity (and so energy generation rate) can be approximated as $\kappa_y \sim v_e l_e$, where v_e is the root-mean-square meridional barotropic eddy velocity and l_e is the meridional eddy scale; 2) the horizontal eddy scale is approximately the Rhines scale $l_e \sim (v_e/\beta)^{1/2}$; and 3) the upscale energy flux, eddy scale, and eddy velocity are related by Taylor's estimate $v_e^3/l_e \sim \kappa_y \lambda^2 U^2$. Together these lead to the estimates $v_e \sim \lambda^2 U^2/\beta$, $l_e \sim \lambda U/\beta$, and $\kappa_y \sim \lambda^3 U^3/\beta^2$.

In the special case that $U = 0$, Spall (2000) alters the Held and Larichev theory by assuming that, while barotropic eddies still have a typical meridional scale given by the Rhines scale, the mixing length l_e instead scales with the zonal width of the domain L_x . Spall motivates this choice by arguing that baroclinic potential vorticity can develop arbitrarily long zonal anomalies without being influenced by β . Using the definitions above, this amounts to assuming 1) $\kappa_x \sim v_e L_x$, 2) $v_e^3/l_e \sim \kappa_x \lambda^2 V^2$, and, as before, 3) $l_e \sim (v_e/\beta)^{1/2}$. The predicted estimates are thus $v_e \sim (\lambda^4 V^4 L_x^2/\beta)^{1/3}$, $l_e \sim (\lambda^2 V^2 L_x/\beta^2)^{1/3}$, and $\kappa_x \sim L_x (\lambda^4 V^4 L_x^2/\beta)^{1/3}$.

The dramatic increase of eddy energy with increasing β found by Arbic and Flierl (2004a), as well as the fact that a steady state can be obtained without boundaries ($L_x \rightarrow \infty$), demands that we seek an alternate mechanism for the zonal eddy length scale. Returning to the passive scalar analogy, which should hold all the more at high eddy energy levels, energy generation in the $U = 0$ case results from the passive transport of eddy baroclinic PV by the jet-dominated barotropic eddy flow u_ψ . Following Taylor (1920), one can relate the eddy transport, or effective eddy diffusivity, to the velocity correlation. In a perfectly smooth jet, the velocity correlation between two neighboring particles (in the cross-stream direction) would grow linearly with time to infinity, so the diffusivity would diverge. When the

jet is embedded in a turbulent background, as in the present problem, there is some length scale over which particles will be swept apart by the jet, but then decorrelated by the turbulent background, and this is the effective mixing length. The effective eddy diffusivity in the along-jet direction will thus increase as the background turbulent diffusivity decreases. This is the shear-dispersion problem of Taylor (1953) (see also Young et al. 1982).

Smith (2005) considered the system (2.3) with F_τ replaced by a small-scale random forcing (with total upscale energy generation g) and derives predictions for the diffusivities κ_x and κ_y in β -plane turbulence. It is shown therein that the best estimate for the background turbulent diffusivity (the cross-jet diffusivity κ_y) is the Held and Larichev estimate (see also Smith et al. 2002; Barry et al. 2002)

$$\kappa_y \approx (g^3/\beta^4)^{1/5}. \quad (2.4)$$

The along-jet effective diffusivity is found by considering a tracer χ with a zonal mean gradient stirred by β -plane turbulence, and approximating its dynamics with an advection-diffusion equation for a large-scale, periodic, smooth jet flow $\mathbf{u} = U_{\text{jet}}(y)\mathbf{i}$ and a turbulent diffusivity κ_y , is written

$$\frac{\partial \chi}{\partial t} - \kappa_y \frac{\partial^2 \chi}{\partial y^2} - U_{\text{jet}}(y), \quad (2.5)$$

where we have used the linearity of the tracer equation to set $\partial \overline{\chi} / \partial x = 1$ without loss of generality. The equilibrated along-jet diffusivity $\kappa_x = \lim_{t \rightarrow \infty} -\overline{U_{\text{jet}} \chi}$ takes on the constant value

$$\kappa_x = \kappa_y^{-1} \sum_{n=-\infty}^{\infty} \frac{|\hat{U}_n|^2}{k_n^2}, \quad (2.6)$$

where \hat{U}_n are the Fourier components of U_{jet} , and $k_n = n\pi/L$ are the wavenumbers, such that

$$U_{\text{jet}}(y) = \sum_{n=-\infty}^{\infty} \hat{U}_n e^{-ik_n y}.$$

The derived along-jet diffusivity increases with decreasing κ_y and in fact diverges in the limit $\kappa_y \rightarrow 0$, in support of the expectations from the thought experiment.

The next obvious thing to do is incorporate this result into the scaling for the energy generation in the closure theory by assuming a sinusoidal jet flow. Before proceeding, we test the underlying idea of a shear-dispersion energy generation mechanism in a set of numerical experiments.

3. Numerical experiments

In this section the results of a set of numerical simulations using a standard two-layer spectral quasigeostrophic model are described. The model has equal layer depths and a maximum resolved wavenumber of $k_{\max} = 127$. Nonlinear terms are calculated using the method of (Orszag 1971), with isotropic truncation at $(8/9)k_{\max}$, and physical space fields are represented on a 256^2 grid. The enstrophy cascade is absorbed by an exponential cutoff filter that acts only on wavenumbers $k > k_{\text{cut}} = 90$ [though the effective scale at which dissipation becomes active is even smaller; see Smith and Vallis (2002), Smith et al. (2002), for model details]. The domain is 2π periodic, so that the $k = 1$ wave fills the domain, and the deformation wavenumber is fixed at $\lambda = 40$ for some runs and $\lambda = 60$ for others. All simulations have $U = 0$ and $V = 0.1$ (nondimensional units) so that the Eady time scale is $(V\lambda)^{-1} = 0.25$. The control parameters explored are the nondimensional Coriolis gradient $\tilde{\beta} = \beta/(\lambda^2 V)$ and the nondimensional bottom drag $\tilde{r} = r/(\lambda V)$.

As discussed originally by Haidvogel and Held (1980), in the homogeneous limit, these are the only parameters of the problem. Each simulation was first spun up to steady state and, at that point, a passive tracer was added to each simulation. The passive tracer was stirred only by the barotropic velocity, and its variance was generated by a linear, meridional mean gradient. The tracer acts as an independent measure of the meridional diffusivity κ_y . Specifically, the modeled tracer is

$$\partial_t \phi + \mathbf{u}_{\text{bt}} \cdot \nabla \phi + v_{\text{bt}} = D_\phi,$$

where \mathbf{u}_{bt} is the barotropic velocity and D_ϕ is the dissipation (modeled using an exponential cutoff filter similar to that for vorticity), so the diffusivity in the meridional direction is

$$\kappa_y = -\overline{v_{\text{bt}} \phi}, \quad (3.1)$$

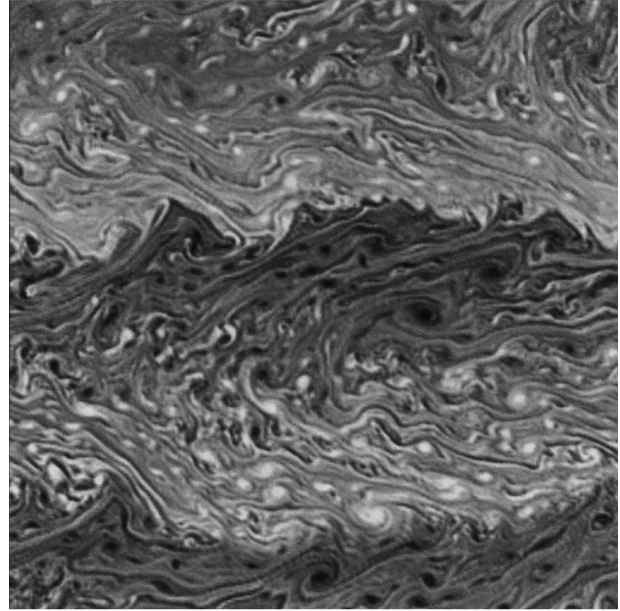
where, as with the equation for χ , we have set $\partial \bar{\phi} / \partial y = 1$.

Thirty simulations were completed and included in the analysis with the intention of covering a wide swath of \tilde{r} - $\tilde{\beta}$ parameter space. An even larger set would have been performed, and at higher resolution, but for the fact that in the most interesting part of parameter space ($\tilde{r} < 1$), up to 2×10^7 time steps were required to achieve equilibration for some simulations, and no simulation in the set took less than 10^6 timesteps.

a. Results

Results from a prototypical simulation with $\tilde{r} = 0.3$ and $\tilde{\beta} = 6.25$ (i.e., relatively small drag and large β) are

(a)



(b)

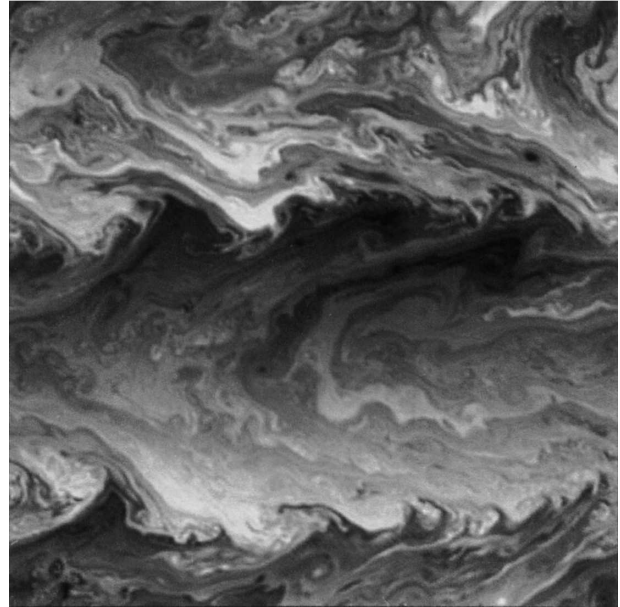


FIG. 1. (a) Vorticity field for simulation with $\tilde{r} = 0.3$ and $\tilde{\beta} = 6.25$. (b) Tracer stirred by barotropic mode of same simulation.

shown in Figs. 1 and 2. In the former, snapshots of the physical space vorticity and tracer fields are shown. Both fields demonstrate the presence of two fronts, consistent with the wavenumber-2 barotropic kinetic energy peak seen in Fig. 2b. Figure 2a of the latter shows the spinup of the barotropic kinetic and total potential energy. Apparently, the total energy is $\sim 6 \times 10^6$ times that of the background flow and is dominated

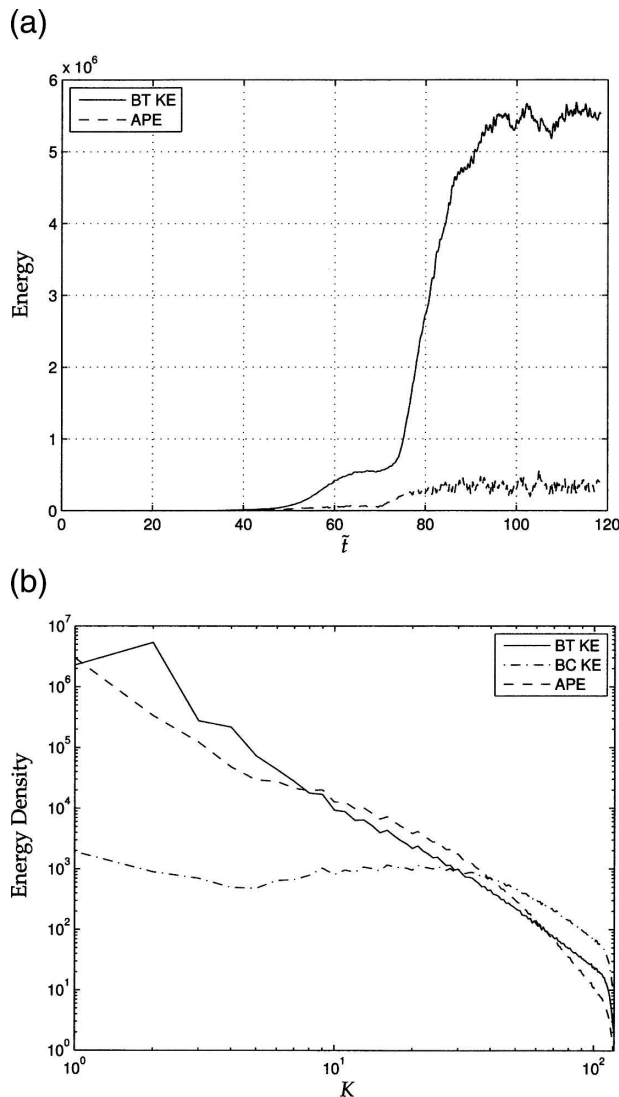


FIG. 2. (a) Time series of barotropic kinetic energy (solid) and available potential energy (dashed) for simulation with $\tilde{\tau} = 0.3$ and $\tilde{\beta} = 6.25$. Time is in units $(\lambda V)^{-1}$ and energy is nondimensionalized by V^2 . (b) Spectra of barotropic kinetic energy (solid), baroclinic kinetic energy (dash-dotted) and available potential energy (dashed) for same simulation.

by barotropic kinetic energy.² On the other hand, considering again the spectra in Fig. 2b, the potential energy is accumulated at the domain scale.

Typically, energy at the domain scale means that one should rerun the simulation with different parameters

² The length of the equilibrated portion of the run may worry some readers; B. Arbic (2005, personal communication), however, ran a simulation using the same parameters for much longer, and found that this energy level remains nearly constant for long times.

such that the energy peaks are well-separated from the domain scale. Strikingly, the entire series of simulations performed at this value of drag ($\tilde{\tau} = 0.3$) produced barotropic kinetic energy peaks at $K = 2$ (Fig. 3) and potential energies at the domain scale (not shown). The reasons for this will be discussed below, in the context of the scaling theory.

Runs with higher drag equilibrate with weaker energy and more jets, hence a smaller energy-containing scale. At large drag and small β , such as in the simulation with $\tilde{\tau} = 1$ and $\tilde{\beta} = 0.625$, no jets form. This is the f -plane limit with eddy statistics controlled entirely by the drag (Arbic and Flierl 2004b; Thompson and Young 2006).

The key quantity of interest in all these simulations is the eddy generation, $V^2 \lambda^2 \kappa_x$ (when $U = 0$ as is the case in the simulations discussed here). Nondimensionalizing the diffusivity using λ^{-1} as a length scale and $(V\lambda)^{-1}$ as a time scale, $\tilde{\kappa}_x = \lambda V^{-1} \kappa_x$. The values of $\tilde{\kappa}_x$ for each simulation are plotted as a two-dimensional function of $\tilde{\tau}$ and $\tilde{\beta}$ in Fig. 4. The data do not fall neatly onto some obvious functional surface, but do exhibit some clear dependencies. Notably, at low drag and high β , the generation rate is orders of magnitude larger than that at high drag and low β . It also appears that there is a sharp transition dependent on $\tilde{\tau}$. This is consistent with the expectation that, in the limit of large drag, one should find a flow that reverts to the f -plane limit mentioned above, with drag halting the cascade at small enough scales that β cannot act to elongate the zonal flow. Still, at any $\tilde{\tau}$, if $\tilde{\beta}$ is made large enough, one should again find β -dominated flow and higher energies. This is apparent in the solution.

The fundamental question of the mechanism for the generation of eddy energy was assessed by applying (2.6) directly to each simulation. Specifically, for each steady-state simulation, the meridional diffusivity κ_y is calculated from the passive tracer using (3.1), and the spectral components \hat{U}_n and k_n are calculated from the Fourier transform of the zonal and short-time average zonal velocity at a range of times. Thus, independent of the feedback mechanisms that generated the steady-state flow, the predicted energy generation is calculated directly from the flow and compared to the measured generation. For the simulation described above with $\tilde{\tau} = 0.3$ and $\tilde{\beta} = 6.25$, the measured and predicted diffusivities are plotted as functions of time in Fig. 5a. The predicted solution tracks the measured diffusivity, but with a constant positive offset of about 20%. The time-averaged predicted zonal diffusivity for all simulations are plotted against measured values in Fig. 5b, demonstrating that the shear-dispersion hypothesis is fundamentally and robustly correct.

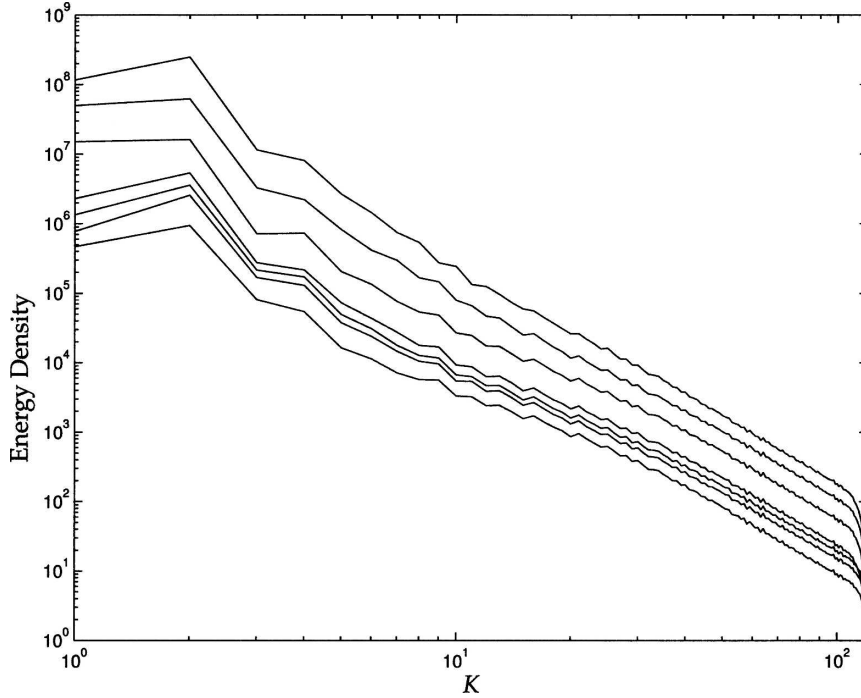


FIG. 3. Barotropic kinetic energy spectra for the set of simulations with $\lambda = 40$ and $\bar{r} = 0.3$. Values of Coriolis gradient (from lowest energy to highest) are $\tilde{\beta} = 3.125, 5.0, 6.25, 7.5, 12.5, 25.0, 50.0$. Remarkably, the peak energy scale does not change over more than a decade of change in β .

b. Scaling theory

To close the problem, we need independent predictions for the two diffusivities, the eddy length scale and the eddy velocity. We will consider each assumption separately and test them against the numerical results where possible.

1) DIFFUSIVITY PREDICTIONS

First, we can immediately test the Held and Larichev prediction (2.4). Figure 6a plots $\tilde{\kappa}_y$ against the predicted value, using the generation rate produced by the model for each simulation. The fit is not exact but demonstrates that the scaling is roughly correct, consistent with past studies. The values calculated from the numerical experiments also show that the meridional diffusivities are many orders of magnitude smaller than the zonal diffusivities, rationalizing the neglect of zonal mean shear in this research. Simulations with both flow components present have been performed, but are not included here—these simulations demonstrate that the contribution of zonal flow instabilities is negligible in the small- to medium-drag limit.

To make a closed prediction for the zonal diffusivity, we consider the simplest possible jet structure

$$u_{\text{jet}}(y) = \hat{U}_0 \sin(k_{\text{jet}}y + \alpha),$$

where α is an arbitrary constant phase, \hat{U}_0 is the maximum jet speed, and k_{jet} is the meridional wavenumber of the jet. The along-jet diffusivity (2.6) in this case simplifies to

$$\kappa_x = \frac{\hat{U}_0^2}{2\kappa_y k_{\text{jet}}^2} = \frac{U_{\text{jet}}^2}{\kappa_y k_{\text{jet}}^2}, \tag{3.2}$$

where $U_{\text{jet}} = (\overline{u_{\text{jet}}^2})^{1/2} = \hat{U}_0/2^{1/2}$. We can check this estimate directly against the model results by estimating U_{jet} as the zonal and time average of the zonal velocity and again using the values of κ_y measured from the passive tracer, given by (3.1). The results are plotted in Fig. 6b. Particularly for larger values of $\tilde{\kappa}_x$, this estimate does a remarkably good job at describing the results.

Substituting the expression (2.4) for κ_y into (3.2), setting $g = \lambda^2 V^2 \kappa_x$, and solving for κ_x we have the nondimensional result

$$\tilde{\kappa}_x = \left(\frac{\tilde{U}_{\text{jet}}}{\tilde{k}_{\text{jet}}} \right)^{5/4} \tilde{\beta}^{1/2}. \tag{3.3}$$

This prediction is plotted against the measured zonal diffusivity in Fig. 7. Apart from the simulation with the smallest value, this expression is better than even the raw calculation of (2.6) shown in Fig. 5. The author can find no apparent reason that expression (3.3), in which

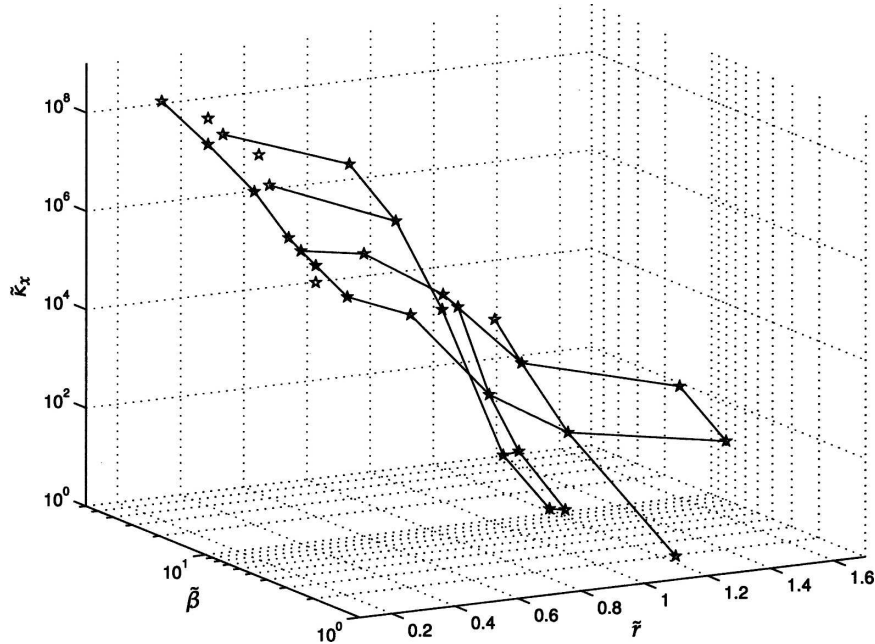


FIG. 4. Nondimensional energy generation, or zonal diffusivity $\tilde{\kappa}_x = \kappa_x \lambda V^{-1}$, for each simulation, plotted as a function of β and \bar{r} . Some connecting lines are plotted to aid in visualization of the results.

κ_y , has been eliminated using the Held and Larichev prediction and the assumed structure of the jets has been simplified, should fit the data so well.

2) ENERGY CONSTRAINT

The presence of linear drag on the bottom layer vorticity affords us a constraint on the total energy generation

$$\lambda^2 V^2 \kappa_x \approx \frac{r}{2} (\overline{|\nabla\psi|^2} + \overline{|\nabla\tau|^2} - 2\overline{\nabla\psi \cdot \nabla\tau}), \quad (3.4)$$

where we have neglected the small-scale dissipation term. Thompson and Young (2006) derive a new conservation law for the cross term, which in steady state implies that³ $\overline{\nabla\psi \cdot \nabla\tau} = \overline{|\nabla\tau|^2}$. Thus to a good approximation we can write

$$g \approx \frac{r}{2} (\overline{|\nabla\psi|^2} - \overline{|\nabla\tau|^2}).$$

Since all of the simulations satisfy the assumption of large scales (compared to the deformation scale), we can safely neglect the baroclinic kinetic energy term and write

³ Note that the factor of $\sqrt{2}$ in (35) of Thompson and Young (2006) is due to a different definition of the baroclinic mode than that used here.

$$E_{bt} \equiv \frac{1}{2} \overline{|\nabla\psi|^2} \approx r^{-1} g. \quad (3.5)$$

The two sides of this equation are plotted against one another in Fig. 8. The fit is remarkably good.

3) SEPARATING JETS FROM TURBULENCE

To apply the shear-dispersion generation prediction, we need to separate the jets from the turbulence in the barotropic mode and so write

$$\frac{1}{2} U_{jet}^2 + E_{turb} \approx r^{-1} g. \quad (3.6)$$

At this point we are still in good shape, but now must make independent estimates of the two terms on the left-hand side. Smith et al. (2002) show that the turbulent energy of two-dimensional, β -plane flow in the small-drag limit is nearly independent of drag. Smith [2005, (4.3)] uses this result to make the estimate

$$E_{turb} \approx \frac{3}{2} (C^6 g^4 \beta^{-2})^{1/5}, \quad (3.7)$$

where $C \approx 6$ is a Kolmogorov constant. The numerical value of the turbulent barotropic energy for each simulation is plotted against this estimate in Fig. 9. Apparently this is not particularly accurate, perhaps because of the assumption of independence from drag (which is

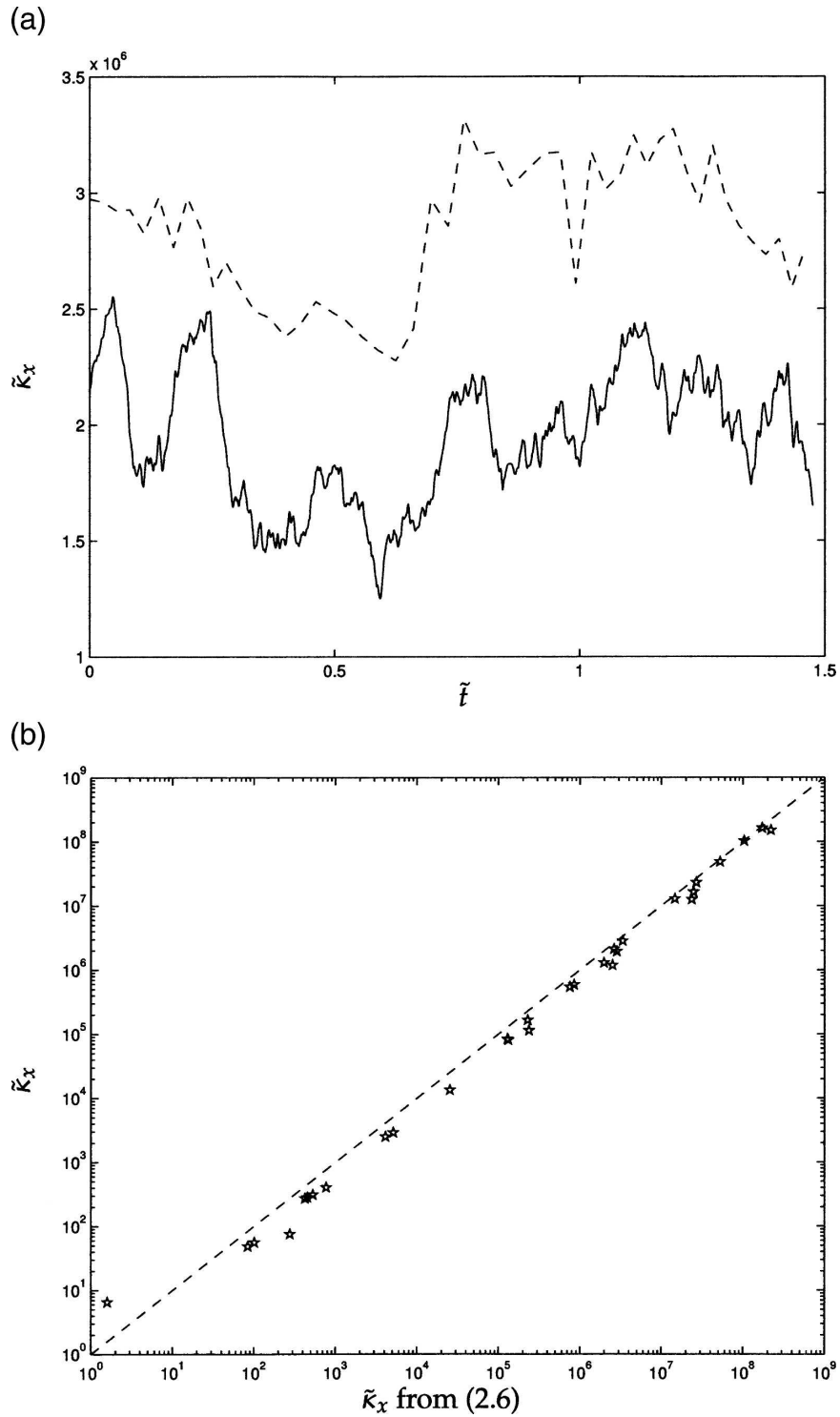


FIG. 5. (a) Nondimensional energy generation, or zonal diffusivity $\kappa_x = \kappa_x \lambda V^{-1}$, for simulation with $\tilde{\tau} = 0.3$ and $\tilde{\beta} = 6.25$ (solid) and shear-dispersion prediction calculated directly from flow field using (2.6) (dashed). The prediction is systematically too high, but tracks the solution. (b) The $\tilde{\kappa}_x$ for each simulation, plotted against same calculation as in (a), but averaged in time.

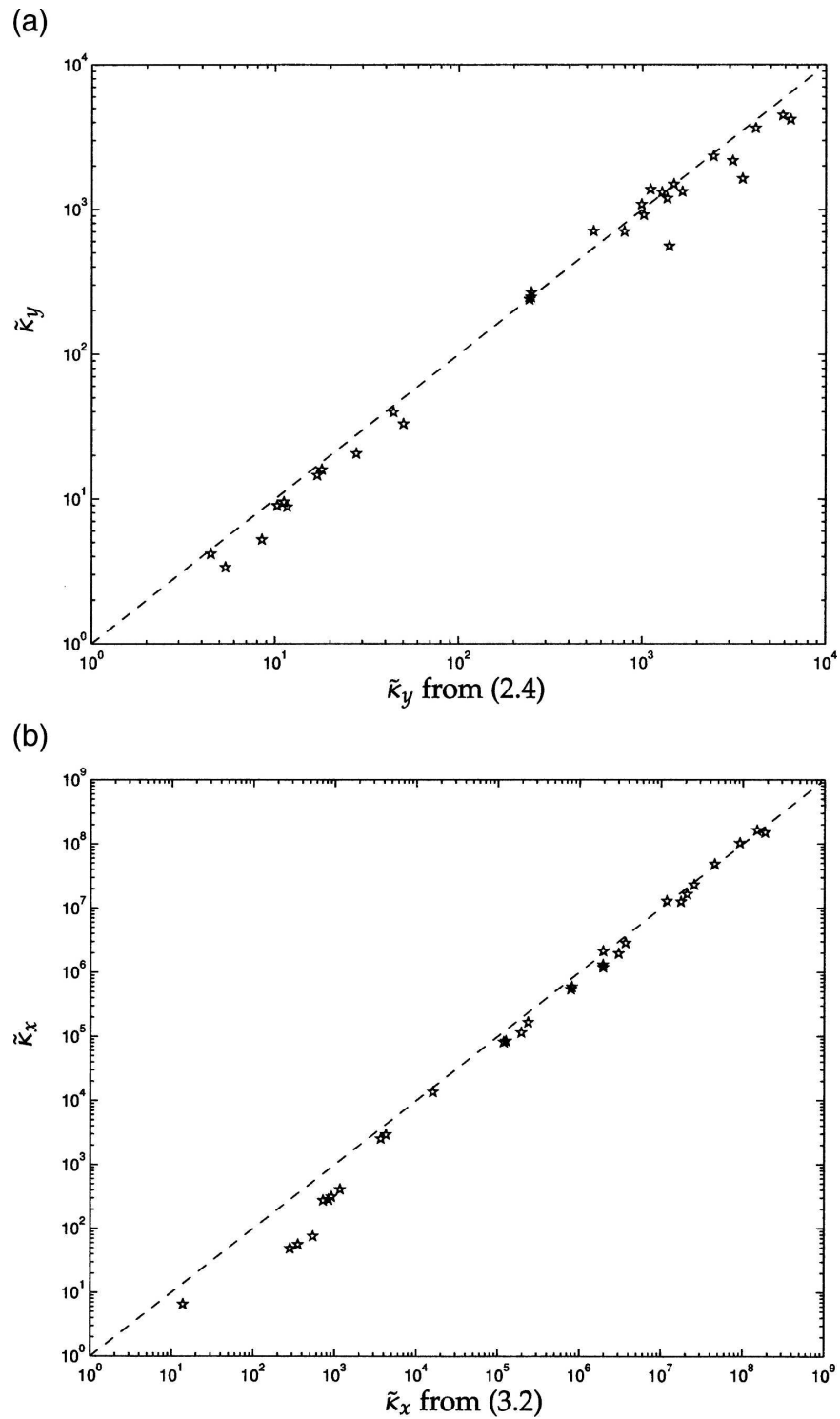


FIG. 6. (a) Nondimensional meridional diffusivity $\tilde{\kappa}_y$ for each simulation plotted against its theoretical prediction (2.4). (b) Nondimensional energy generation, or zonal diffusivity $\tilde{\kappa}_x = \kappa_x \lambda V^{-1}$, for each simulation, plotted against the theoretical estimate (3.2), based on the assumption of sinusoidal jets.

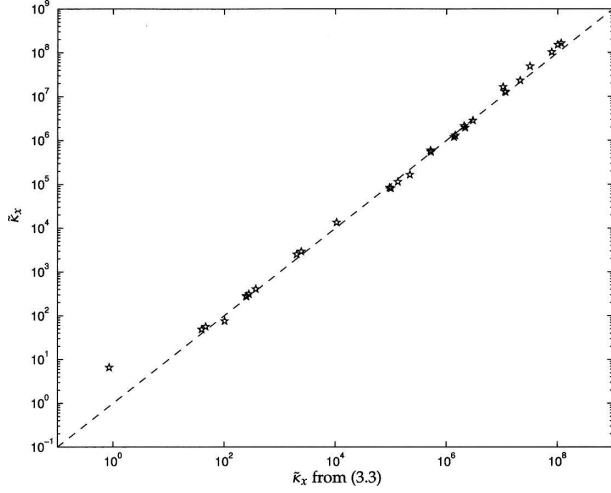


FIG. 7. Nondimensional energy generation or zonal diffusivity \bar{k}_x plotted against prediction (3.3), combining shear-dispersion prediction for zonal diffusivity and turbulent diffusion for meridional diffusivity.

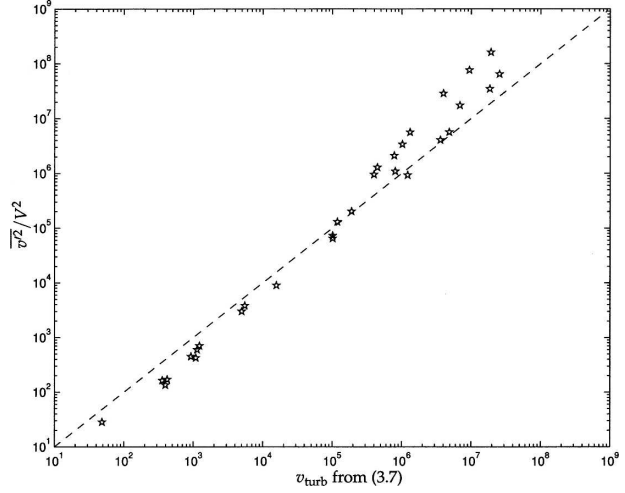


FIG. 9. Turbulent (nonjet) barotropic kinetic energy, estimated as $(1/2)[(u - U_{\text{jet}})^2 + v^2]$, plotted against predicted value from integration of Kolmogorov spectrum, (3.7).

harder to justify in the present baroclinic case), and things only get worse from here.

One can attempt to relate the jet energy to the jet scale via the Rhines relation, calculated as in Smith et al. (2002) as the integral of the putative -5 spectrum (see, e.g., Chekhlov et al. 1996; Smith et al. 2002)

$$\frac{1}{2} U_{\text{jet}}^2 \approx a \beta^2 k_{\text{jet}}^{-4}, \quad (3.8)$$

where $a \approx 0.1$. Considering Fig. 10, for the system at hand this is the poorest approximation yet. Figure 10a plots the nondimensionalized version of (3.8) di-

rectly, and Fig. 10b plots $1/k_{\text{jet}}$ against the Rhines scale $\sqrt{\beta/U_{\text{jet}}}$. Neither a plausible explanation of this result nor a better theory for the jets is apparent to the author.

4) CLOSURE

Despite the imperfections of the last two relations, one might attempt to put the above relations together to close for the diffusivity, or eddy energy generation rate. However, if one puts the relations together, the resulting prediction actually has the generation decreasing with increasing β , just the opposite of what is found in the simulations. Therefore, given the accuracy of the predictions for the diffusivities and for the barotropic energy budget, the Rhines relationship cannot be correct in this particular system.

Moreover, for simulations with small drag, which have their energy near the domain scale, it seems that the unavoidable conclusion, given that in this regime the stopping scale is nearly constant with β , is that the cascade cannot be controlled by β and that some additional mechanism is necessary. Given that the available potential energy is always at the domain scale in these simulations, even though the kinetic energy is not, perhaps thermal drag would close the system. This is left for future work.

Note in passing that, if one assumes small drag and takes k_{jet} to be constant, the closed solution does yield a diffusivity and a jet velocity that increase with β , as observed. In lieu of a complete closure or understanding of the jet dynamics, this is however not very useful and so is not included.

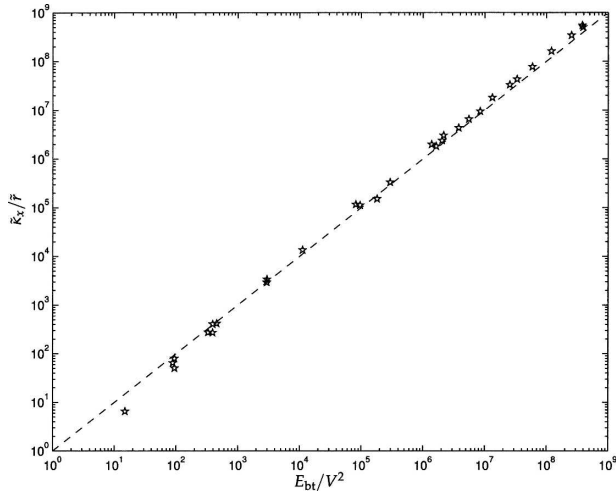


FIG. 8. Nondimensional barotropic kinetic energy E_{bt}/V^2 for each simulation plotted against the estimate \bar{k}_x/\bar{F} ; see (3.5).

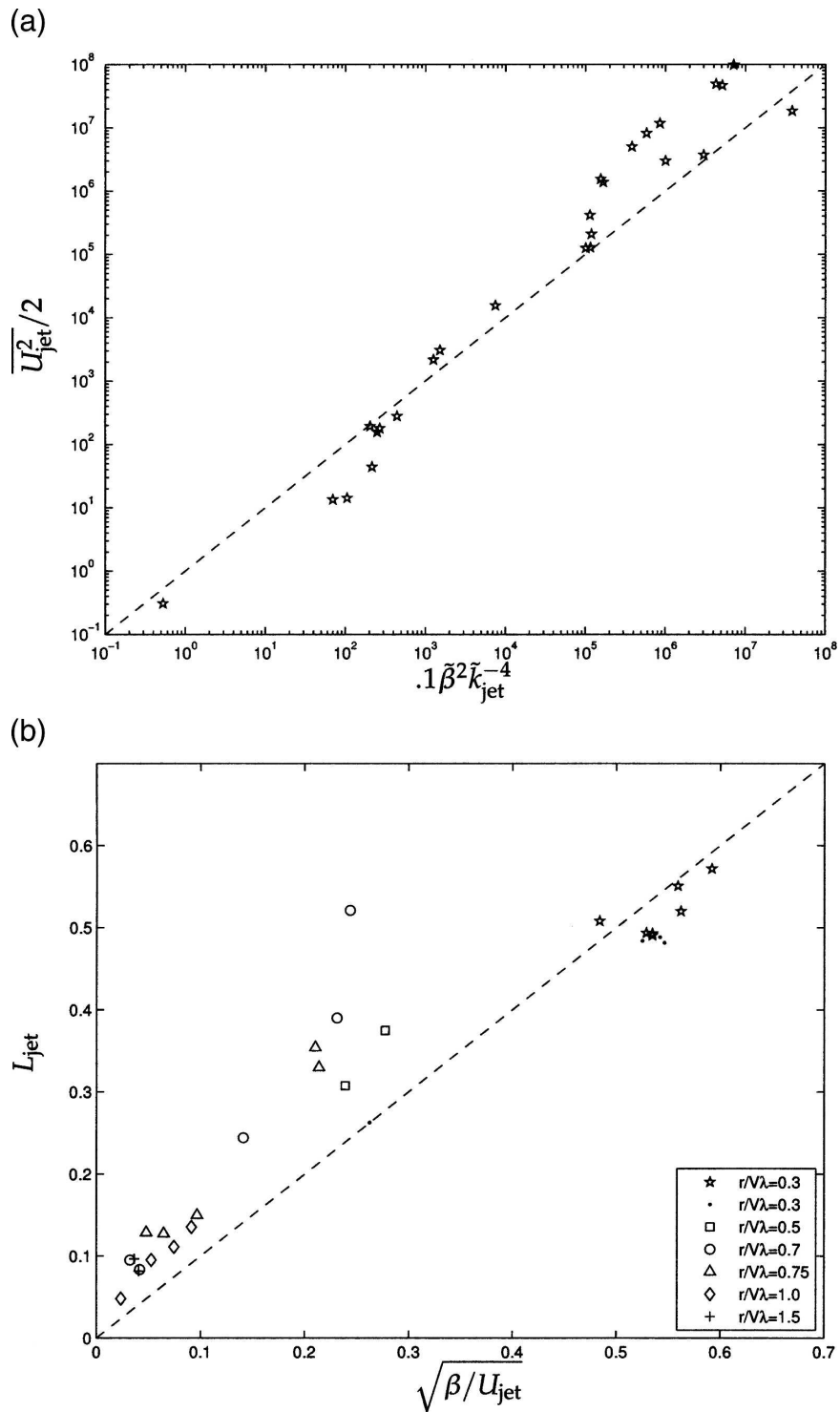


FIG. 10. (a) Nondimensional jet energy $\overline{U_{jet}^2}/2V^2$ plotted against $1\tilde{\beta}^2\tilde{k}_{jet}^4$. (b) Same relation used to plot $L_{jet} = 1/k_{jet}$ against the Rhines scale. In both cases, the jet wavenumber is calculated as the peak of the meridional barotropic energy spectrum.

4. Discussion and conclusions

Numerical simulations of the two-layer model with a mean background shear directed along the mean vorticity gradient (the pure nonzonal flow problem) demonstrate a host of behaviors that are qualitatively different from the zonal mean flow problem to a remarkable degree. The root of the distinction between the two limits is the nature of the eddy generation, and in particular its interaction with jets that arise in the flow due to β . Nonzonal mean shear leads to eddy generation driven by correlations with the zonal eddy velocity and the baroclinic potential vorticity. When jets are present, this eddy flux is best described by a shear-dispersion model. The result is primarily that the eddy energy in the nonzonal flow case is orders of magnitude larger than that in the zonal flow problem and, moreover, that the energy and the generation rate increase with increasing β , just the opposite of the behavior in the zonal flow case.

When the drag parameter $r/\lambda V$ is small compared to unity, a strong feedback arises in the jet scale. On the one hand, increasing β leads to faster Rossby waves, so for fixed eddy turn-around time jets should form at smaller scale. But the turbulent time scale is not fixed since as β is increased the eddy generation and hence energy increase, driving a faster turbulent time scale and a more vigorous inverse cascade. These two effects work against each other and lead to a balance at some length scale that, at least in the presently discussed simulations, is apparently invariant with β . It could be the case that an even larger separation between the domain scale and the deformation scale would lead to an observed variation of the jet-scale with β at low drag since the former turns out to be so near the domain scale in the present simulations. However, the same results are obtained when the deformation wavenumber is increased from 40 to 60 at $\tilde{r} = 0.3$, so this seems unlikely.

One could interpret the lack of separation between the eddy and domain scale in the small-drag limit as supporting the theory proposed by Spall (2000). Alternatively, one could ask whether sufficiently high drag could yield a local limit in Spall's calculations. Most of the simulations presented by Spall used a sponge layer at the western boundary to dissipate energy, but in one set a weak linear bottom drag is also included. The result is that the overall eddy energy is reduced, and the scaling theory provides a less accurate description at high eddy energies, implying some dependence on drag not accounted for by the theory. Therefore, one might conclude that drag and domain effects are at least in competition in his experiments. Using (3.2), we can

compute the effective zonal eddy length scale. Setting $\kappa_x = l_e u_e$, and taking $u_e = U_{\text{jet}}$, we have that $l_e = U_{\text{jet}} L_{\text{jet}}^2 / \kappa_y$. Using ballpark estimates $U_{\text{jet}} \sim 5 \text{ cm s}^{-1}$, $L_{\text{jet}} = 300 \text{ km}$, and $\kappa_y = 1000 \text{ m}^2 \text{ s}^{-1}$ we have that $l_e \sim 2200 \text{ km}$, very similar to the domain scale L_x used in Spall (2000).

The incredibly effective eddy energy generation mechanism found in the present idealized problem should lead one to question whether this effect is present in the ocean. Observed midocean eddy velocities are much stronger than mean shears, but not by two or more orders of magnitude. Either bottom drag must not be small, as hypothesized by Arbic and Flierl (2004a), or some other dissipation mechanism must act to quell eddy energy. Quadratic bottom drag is a more truthful representation of the effects of a bottom boundary layer on the interior flow and is also naturally scale-selective (Griani et al. 2004). One could also argue that a direct sink on eddy available potential energy, such as thermal drag, should be included. Unbalanced flows have also been entirely neglected.

A full closure for the problem was not obtained, due to the difficulty in finding a suitable theory for the jet scale—the Rhines scale is a poor predictor of the jet scales that evolved in these simulations. At small drag, this is likely related to the feedback discussed above, but the Rhines scaling is also inaccurate at large drag. It may not be a worthwhile pursuit to attempt to close the present system since, as pointed out, the energies are too large to be relevant to the ocean without a very strong dissipation mechanism. Moreover, the energy generation is so large that surely the instability will not remain localized and so the homogeneous, local limit may not apply.

The aspect of the problem that is potentially most useful for future research is the unique eddy energy generation mechanism demonstrated here. Regardless of their genesis and maintenance, jets and elongated eddies lead to shear dispersion of baroclinic potential vorticity that, in the presence of even a weak cross-jet mean shear, leads to intense eddy energy growth.

Acknowledgments. The author thanks Brian Arbic, Mike Spall, and an anonymous referee for helpful comments and a thorough review. The author acknowledges the support of National Science Foundation Grant OCE-0327470. The simulations were performed on the NYU high-performance computer cluster, Max, funded in part by the Office of Naval Research.

REFERENCES

- Arbic, B. K., and G. R. Flierl, 2004a: Effects of mean flow direction on energy, isotropy, and coherence of baroclinically un-

- stable beta-plane geostrophic turbulence. *J. Phys. Oceanogr.*, **34**, 77–93.
- , and —, 2004b: Baroclinically unstable geostrophic turbulence in the limits of strong and weak bottom Ekman friction: Application to midocean eddies. *J. Phys. Oceanogr.*, **34**, 2257–2273.
- Barry, L., G. C. Craig, and J. Thurnburn, 2002: Poleward heat transport by the atmospheric heat engine. *Nature*, **415**, 774–777.
- Charney, J., 1947: Dynamics of long waves in a baroclinic westerly current. *J. Meteor.*, **4**, 135–162.
- Chekhlov, A., S. A. Orszag, S. Sukoriansky, B. Galperin, and I. Staroselsky, 1996: The effect of small-scale forcing on large-scale structures in two-dimensional flows. *Physica D*, **98**, 321–334.
- Griani, N., I. M. Held, K. S. Smith, and G. K. Vallis, 2004: The effects of quadratic drag on the inverse cascade of two-dimensional turbulence. *Phys. Fluids*, **16**, 1–16.
- Haidvogel, D. B., and I. M. Held, 1980: Homogeneous quasi-geostrophic turbulence driven by a uniform temperature gradient. *J. Atmos. Sci.*, **37**, 2644–2660.
- Held, I. M., and V. D. Larichev, 1996: A scaling theory for horizontally homogeneous, baroclinically unstable flow on a beta-plane. *J. Atmos. Sci.*, **53**, 946–952.
- Larichev, V. D., and I. M. Held, 1995: Eddy amplitudes and fluxes in a homogeneous model of fully developed baroclinic instability. *J. Phys. Oceanogr.*, **25**, 2285–2297.
- Maximenko, N. A., B. Bang, and H. Sasaki, 2005: Observational evidence of alternative zonal jets in the world ocean. *Geophys. Res. Lett.*, **32**, L12607, doi:10.1029/2005GL022728.
- Nadiga, B. T., 2006: On zonal jets in oceans. *Geophys. Res. Lett.*, **33**, L10601, doi:10.1029/2006GL025865.
- Orszag, S. A., 1971: Numerical simulation of incompressible flows within simple boundaries: Accuracy. *J. Fluid Mech.*, **146**, 21–43.
- Pedlosky, J., 1987: *Geophysical Fluid Dynamics*. 2d ed. Springer, 710 pp.
- Rhines, P. B., 1975: Waves and turbulence on a β -plane. *J. Fluid Mech.*, **69**, 417–443.
- Richards, K. J., N. A. Maximenko, F. O. Bryan, and H. Sasaki, 2006: Zonal jets in the Pacific Ocean. *Geophys. Res. Lett.*, **33**, L03605, doi:10.1029/2005GL024645.
- Robinson, A., and J. McWilliams, 1974: The baroclinic instability of the open ocean. *J. Phys. Oceanogr.*, **4**, 281–294.
- Salmon, R., 1980: Baroclinic instability and geostrophic turbulence. *Geophys. Astrophys. Fluid Dyn.*, **10**, 25–52.
- Smith, K. S., 2005: Tracer transport along and across coherent jets in two-dimensional turbulent flow. *J. Fluid Mech.*, **544**, 133–142.
- , and G. K. Vallis, 2002: The scales and equilibration of mid-ocean eddies: Forced-dissipative flow. *J. Phys. Oceanogr.*, **32**, 1699–1721.
- , G. Boccaletti, C. C. Henning, I. N. Marinov, C. Y. Tam, I. M. Held, and G. K. Vallis, 2002: Turbulent diffusion in the geostrophic inverse cascade. *J. Fluid Mech.*, **469**, 13–48.
- Spall, M. A., 2000: Generation of strong mesoscale eddies by weak ocean gyres. *J. Mar. Res.*, **58**, 97–116.
- Taylor, G. I., 1920: Diffusion by continuous movements. *Proc. London Math. Soc.*, **20** (2), 196–212.
- , 1953: Dispersion of soluble matter in solvent flowing slowly through a tube. *Proc. Roy. Soc. London*, **A219**, 186–203.
- Thompson, A. F., and W. R. Young, 2006: Scaling baroclinic eddy fluxes: Vortices and energy balance. *J. Phys. Oceanogr.*, **36**, 720–738.
- Vallis, G. K., and M. E. Maltrud, 1993: Generation of mean flows and jets on a beta plane and over topography. *J. Phys. Oceanogr.*, **23**, 1346–1362.
- Walker, A., and J. Pedlosky, 2002: Instability of meridional baroclinic currents. *J. Phys. Oceanogr.*, **32**, 1075–1093.
- Williams, G. P., 1978: Planetary circulations: 1. Barotropic representation of Jovian and terrestrial turbulence. *J. Atmos. Sci.*, **35**, 1399–1426.
- Young, W. R., P. B. Rhines, and C. J. R. Garrett, 1982: Shear-flow dispersion, internal waves and horizontal mixing in the oceans. *J. Phys. Oceanogr.*, **12**, 515–527.